

# Persistent homology of quantum entanglement

Bart Olsthoorn<sup>1,\*</sup> and Alexander V. Balatsky<sup>1,2,†</sup>

<sup>1</sup>*Nordita, KTH Royal Institute of Technology and Stockholm University,  
Hannes Alfvéns väg 12, SE-114 21 Stockholm, Sweden*

<sup>2</sup>*Department of Physics, University of Connecticut, Storrs, CT 06269, USA*

(Dated: October 22, 2021)

Structure in quantum entanglement entropy is often leveraged to focus on a small corner of the exponentially large Hilbert space and efficiently parameterize the problem of finding ground states. A typical example is the use of matrix product states for local and gapped Hamiltonians. We study the structure of entanglement entropy using persistent homology, a relatively new method from the field of topological data analysis. The inverse quantum mutual information between pairs of sites is used as a distance metric to form a filtered simplicial complex. Both ground states and excited states of common spin models are analyzed as an example. Beyond these basic examples, we also discuss the promising future applications of this modern computational approach, including its connection to the question of how spacetime could emerge from entanglement.

## I. INTRODUCTION

Problems in quantum physics are often difficult to solve due to an exponentially large Hilbert space (e.g.  $d = 2^N$  for  $N$  spins), which limits exact diagonalization (ED) to small systems only. However, due to the remarkable entanglement scaling properties found in many physical systems, it is often possible to focus only on a small corner of the Hilbert space. For example, the problem of finding a ground state of a one-dimensional local and gapped Hamiltonian can be parameterized efficiently with matrix product states (MPS) [1]. Beyond this class of Hamiltonians, the entanglement properties have also proven useful in projected entangled-pair states (PEPS) [2] and the Multiscale Entanglement Renormalization Ansatz (MERA) [3].

Phases of matter can differ in their entanglement scaling properties, and the critical phase transition is typically a point of special interest. The area law states that the entanglement entropy only depends on the surface between two subregions of the system [4, 5]. The transverse field Ising model (TFIM) exhibits a quantum phase transition from the ferromagnet with area law entanglement that to a paramagnet that also follows an area law. At the quantum critical point (QCP), the entanglement entropy diverges logarithmically with the subsystem size (volume law) [6–8]. A randomly selected state in Hilbert space typically follows a volume law. Another example of a phase transition that is studied through entanglement properties is the many-body localization (MBL) transition [9, 10].

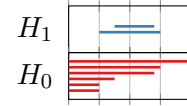
Considering the daunting complexity of Hilbert space, various large scale computational techniques are employed: phase transitions and order parameters are now often analyzed and constructed with machine learning [11, 12]. Persistent homology analysis has been used to

Hilbert space

$|\psi\rangle$

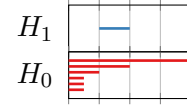
→

Barcode space



$|\varphi\rangle$

→



$\epsilon$

FIG. 1. A given state  $\psi$  in Hilbert space is mapped to a barcode that describes the topological structure of the entanglement of its subsystems. The proximity parameter  $\epsilon$  is computed from the quantum mutual information, and the homology groups indicate features in the emergent geometry.

identify phase transitions in classical spin models [13–16]. These examples also illustrate the evolving views on the importance and unique role that entanglement plays as an indicator of qualitative changes in quantum systems. Our approach focuses on the objects that are derivative of quantum states (simplicial complexes) and function as a key descriptor of global properties of the system. The main technique used in this paper is persistent homology, a relatively new method from the field of topological data analysis (TDA) that computes the shapes present in data [17, 18]. In short, TDA often involves turning a point cloud in data space into a filtered simplicial complex where the filtration is done with a chosen length scale parameter. At each filtration stage, the homology groups are computed and compared. Homology group elements that persist over many stages lead to persistent homology and can be visualized in a barcode or persistence diagram.

In this work, we study the geometric and topological features of the entanglement entropy with persistent homology. The logic of the approach is schematically shown in Fig. 1. A state  $|\psi\rangle$  in Hilbert space is converted to a

\* bartol@kth.se

† balatsky@kth.se

corresponding barcode that efficiently describes its entanglement structure. The barcode is the result of applying persistent homology to a distance matrix that quantifies the entanglement between all subsystems. Using this approach we discuss the changes in barcode space comparing ground states, excited states and phase transitions. As an example, we focus on two common quantum spin chains in a transverse field: Ising model and XXZ model. The former is the simplest example of a quantum phase transition, and the latter is a model commonly used to study many-body localization [10, 19].

The remainder of this paper is structured as follows. In Sec. II we outline how persistent homology captures the entanglement structure of a quantum state. The technical details are presented in Sec. VII and IV. A demonstration is carried out for two different spin models in Sec. V and VI, followed by a discussion in Sec. VII. We conclude in Sec. VIII.

## II. ENTANGLEMENT AND PERSISTENT HOMOLOGY

The foundation of our work is the description of the entanglement structure of a quantum state using persistent homology. Given a state  $|\psi\rangle$ , we divide the quantum system into  $N$  subsystems. For each pair of subsystems, the quantum mutual information  $M_{ij}$  is computed. A structure appears when entangled subsystems (with large mutual information) form clusters. A distance metric is defined as the inverse mutual information between two subsystems. This brings strongly entangled subsystems close while non-entangled subsystems are far apart. Given a distance matrix between all subsystems, the computation of persistent homology groups makes it possible to study topological and geometrical features of the entanglement structure. This information can be plotted as a barcode, where long bars indicate topological features that persist over large length scales. The length scale refers to the entanglement through the defined distance metric. The barcode captures the global entanglement structure of the quantum state and gives a detailed view of the "phase portrait" of the system. How to compute this in practice is outlined in the next section.

The barcode is a summary of the topological and geometrical features of the entanglement structure. Each quantum state has a barcode and it can be used in a number of applications. In our work, we demonstrate that changes in the barcode reveal phase transitions. At the same time, the barcode reveals the length scale of the entanglement in the state which is important when developing suitable wave function ansatz. Finally, the barcode describes the emergent geometry of the entanglement, which could provide a starting point to study the emergence of spacetime from entanglement [20].

The barcodes corresponding to quantum states can be compared in a number of ways. Distance measures such

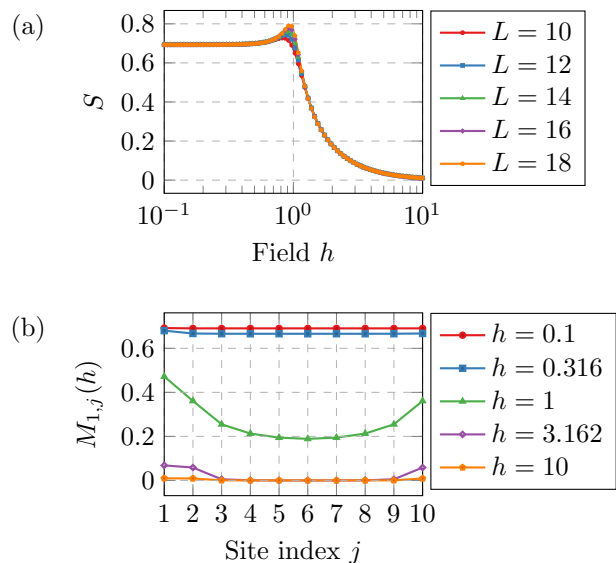


FIG. 2. (a) Entanglement entropy  $S$  as a function of field  $h$  in the 1D TFIM. For small fields  $h$  the entanglement is constant,  $\log(2)$ . At the critical point of  $h = 1$ ,  $S$  grows as  $\log(N)$ . (b) Quantum mutual information between first site 1 and site  $j$  as a function of field  $h$  (logarithmically spaced) in the 1D TFIM. The mutual information  $M_{1j}$  is largest between nearby sites, indicating the local interactions of the Hamiltonian. Periodic boundary conditions are used and lead to increased  $M_{1j}$  for large  $j$ .

as the Bottleneck distance or the Wasserstein distance operate directly on the complete barcodes. However, depending on the application, it can be sufficient to simply count the number of bars at a specific length scale (i.e. the Betti number  $\beta_k$ ). We focus on Betti numbers in our work and demonstrate its sensitivity to quantum phase transitions. However, the computational algorithm outlined here is general and can be used in a variety of applications.

## III. DISTANCE METRIC BASED ON ENTANGLEMENT

The  $N$  particles (or spins) form a discrete point cloud, where the distance metric between spins is the (additive) inverse of the quantum mutual information (MI). Mutual information is commonly used to identify clusters of entanglement, and as a probe for phase transitions (e.g. MBL and quantum phase transitions) [10, 14, 21, 22]. The mutual information between two sites  $i$  and  $j$  is defined as

$$0 \leq M_{ij} = S_i + S_j - S_{ij} \leq 2 \ln 2. \quad (1)$$

Here, the entanglement entropy  $S_i$  and  $S_{ij}$  refer to taking only sites  $i$  and  $i, j$  in subsystem  $A$ , respectively.

**Theorem III.1.** *Let  $D_{ij}$  be the inverse of the MI be-*

tween sites  $i$  and  $j$ ,

$$2 \ln 2 \geq D_{ij} = 2 \ln 2 - M_{ij} \geq 0. \quad (2)$$

This is a distance metric that brings strongly entangled sites ( $M \rightarrow 2 \ln 2$ ) close together ( $D \rightarrow 0$ ), while non-entangled sites ( $M \rightarrow 0$ ) are far apart ( $D \rightarrow 2 \ln 2$ ).

*Proof.* The distance metric defined in Equation 2 satisfies the axioms for a metric because it is symmetric and satisfies the triangle inequality. This triangle inequality relies on properties of quantum entropy, and we start by writing the inequality in terms of entropy,

$$\begin{aligned} D_{xy} &\leq D_{xz} + D_{zy} \\ 2S_z + S_{xy} - S_{xz} - S_{zy} &\leq 2 \ln 2. \end{aligned} \quad (3)$$

In order to show that the inequality holds, we first note that  $S_{xz}$  and  $S_{zy}$  are non-negative and the term  $X = S_{xz} + S_{zy}$  can be replaced by  $S_x + S_y$ , which is guaranteed to be equal or smaller by the strong subadditivity of quantum entanglement (Equation A5). Furthermore, the term  $S_{xy}$  is replaced by an expression that is guaranteed to be larger,  $S_{xy} \leq S_x + S_y$  (Equation A4). This leads to,

$$\begin{aligned} 2S_z + S_x + S_y - S_x - S_y &\leq 2 \ln 2 \\ 2S_z &\leq 2 \ln 2, \end{aligned}$$

which is true because  $S_z$  has a maximum value of  $\ln 2$ . Finally, the distance of point  $i$  with itself,  $D_{ii}$ , is never evaluated when constructing homology, and we can consider it to be zero.  $\square$

Given a set of discrete data (quantum subsystems) and the distance matrix (inverse mutual information), we can now study its homology. Simplicial complexes are a convenient computational platform to form a space and compute its homology using linear algebra. For a practical introduction to persistent homology, see ref [23]. The most important aspects are also introduced in the next section.

#### IV. PERSISTENT HOMOLOGY

In this study, we use Vietoris-Rips filtration using the distance matrix elements  $D_{ij}$  (Equation 2) to form a sequence of simplicial complexes,  $K_1 \subset K_2 \subset \dots \subset K_n$ . For each simplicial complex  $K_i$ , the homology groups  $H_k$  are computed, where  $k$  refers to  $k$ -dimensional simplices (see Fig. 3). The  $k$ -simplices in the complex form  $k$ -chains with  $\mathbb{Z}_2$  coefficients. The boundary operator  $\partial$  gives a sum of the faces of the simplex, where the faces are  $(k-1)$ -simplices. When dealing with  $k$ -chains, the boundary operator is a linear map and  $\partial_k$  indicates the boundary is applied to  $k$ -chains in  $C_k$ . A  $k$ -cycle is a  $k$ -chain with an empty boundary, i.e.  $\partial_k c = 0$ . The homology groups  $H_k$  are defined as the quotient of  $k$ -cycles

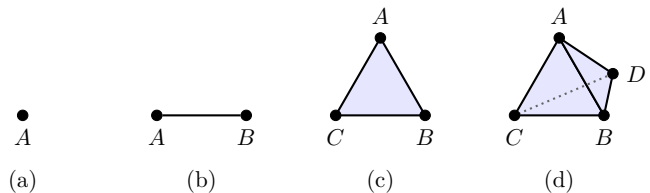


FIG. 3. Entangled quantum subsystems  $A$ ,  $B$ ,  $C$  and  $D$  are represented by simplices. A  $k$ -simplex consists of  $k+1$  subsystems. Here we show (a) 0-simplex (point), (b) 1-simplex (line segment), (c) 2-simplex (filled triangle), (d) 3-simplex (filled tetrahedron). Higher-dimensional simplices exist but are not shown here for simplicity. Simplices are typically glued together to form a simplicial complex and its topological properties are described by simplicial homology.

and  $k$ -boundaries,

$$H_k = \frac{Z_k}{B_k} = \frac{\text{Ker } \partial_k}{\text{Im } \partial_{k+1}}, \quad (4)$$

where  $Z_k$  are the  $k$ -cycles and  $B_k$  the  $k$ -boundaries. The homology groups  $H_k$  are computed for each  $K_i$  and sequences of identical homology lead to so-called persistent homology. The sequence of homology groups are visualized in a persistence barcode or persistence diagram. Both show the same information, and reveal shapes present in the quantum mutual information.

In practical applications, since the barcode itself is not a scalar quantity, it is common to either use scalar properties derived from the barcode or construct a scalar distance between two barcodes. For example, the Betti number is an integer,

$$\beta_k = \text{rank}(H_k) \quad (5)$$

that counts the rank of the  $k$ th homology group. Another example is the lifetime of a specific bar in the barcode. Bars with a long lifetime indicate that a feature (like a 1-dimensional hole) persists over large range of length scale. Features with a short lifetime are sometimes considered to be noise in the input point cloud. However, these features can also indicate the curvature of the manifold that the point cloud was sampled from [24].

In practice, there are many different codes that implement the computation of persistent homology given a distance matrix. We use the GUDHI Python module for the construction of a Vietoris-Rips complex from the distance matrix, and the computation of the barcode [25].

In summary, each state  $|\psi\rangle$  has a set of homology groups and a corresponding barcode. The barcode is a fingerprint of the entanglement structure of the state. Abrupt changes can indicate phase transitions, and barcodes can also differentiate between phases. In general, distances between quantum states can be computed as Bottleneck or Wasserstein distances between corresponding barcodes.

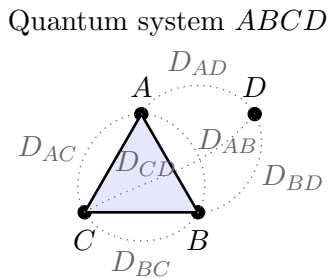


FIG. 4. Example of a simplicial complex created from a quantum system comprising four subsystems:  $A$ ,  $B$ ,  $C$  and  $D$ . The entanglement entropy between all subsystems is used to compute the distance  $D_{ij}$  (Equation 2). This complex corresponds length scale  $\epsilon$ , where in this case subsystems  $A$ ,  $B$  and  $C$  form a 2-simplex. Subsystem  $D$  is not connected to the  $ABC$  component, indicating that the distances between  $D$  and  $A$ ,  $B$  and  $C$  is larger than  $\epsilon$ . Here, the Betti numbers are  $\beta_0 = 2$  (i.e. 2 connected components:  $ABC$  and  $D$ ) and  $\beta_1 = 0$  (no 1-dimensional holes, since the 1-cycle  $ABC$  is also the boundary of the 2-simplex  $ABC$ ).

## V. EXAMPLE 1: ISING CHAIN IN TRANSVERSE FIELD

In order to demonstrate the usefulness of homology, we study the simplest model of a quantum phase transition (QPT), the transverse field Ising model (TFIM) on a one-dimensional lattice. The Hamiltonian  $\mathcal{H}$  of the transverse field Ising model (TFIM) [8],

$$\mathcal{H} = - \sum_i \sigma_i^z \sigma_{i+1}^z - h \sum_i \sigma_i^x, \quad (6)$$

where  $\sigma$  are the Pauli matrices. There is a QPT that can be measured by the magnetization  $M = |1/N \sum_i \sigma_i^z|$ . For  $h = 0$ , the ferromagnetic ground state is the basis state with all spins pointing along the  $z$  direction. For large  $h$ , the ground state is a quantum paramagnet, a superposition of all basis states.

For  $h = 0$ , there is a degenerate ground state that is a product state of all spin up  $|\uparrow\uparrow\dots\uparrow\rangle$  or all down  $|\downarrow\downarrow\dots\downarrow\rangle$ . For a small but finite  $h$ , these levels split with order  $h^N$  and the ground state is a macroscopic superposition  $(|\uparrow\uparrow\dots\uparrow\rangle + |\downarrow\downarrow\dots\downarrow\rangle)$  with  $\ln 2$  entanglement entropy. The system undergoes a quantum phase transition at  $h = 1$ , and the entanglement structure form a 1-cycle, as will be discussed. At  $h = \infty$  the ground state is a quantum paramagnet, i.e. superposition of all basis states  $\frac{1}{\sqrt{2^N}} \sum_i 2^N |i\rangle$ .

Vietoris-Rips complexes are constructed from the distance matrix  $D$ . The barcodes are shown in Figure 5. Regardless of the phase, at  $\epsilon = 2 \ln 2$ , all  $L$  sites are connected, forming a Rips complex with all possible  $(L-1)$ -simplices. At  $\epsilon = 0$ , the sites are all disconnected, leading to a Rips complex of only 0-simplices (points).

Both the low ( $h < 1$ ) and high ( $h > 1$ ) field systems have almost constant mutual information  $M_{ij}$  for all pairs (see Fig. 2). This causes all sites to pair up at the same

length scale in the barcode. However, around the quantum critical point ( $h = 1$ ), neighbouring sites are more strongly entangled, causing a 1-dimensional hole to form inside the ring of spins that persists over a finite length scale. This is a characteristic feature of the critical point.

Due to the symmetry of the Hamiltonian and the periodic boundary conditions, the distances are the same for each site, e.g.  $D_{1,2} = D_{2,3}$ . In the case of  $L \rightarrow \infty$ , the the 1-dimensional hole of the cycle is maximally large. The closure of this hole depends on the longest distance in the chain, the distance between opposite sites. This means that the lifetime of  $H_1$  reaches the maximum possible  $(2 \ln 2 - b)$  as  $L \rightarrow \infty$ . The numerical result in Figure 5(d) shows the lifetime increasing with system size  $L$ , and the birth and death length scales are shown in Fig. 6.

## VI. EXAMPLE 2: XXZ SPIN CHAIN IN TRANSVERSE FIELD

In order to study multiscale entanglement, we now focus on the 1D XXZ spin chain in transverse field with Hamiltonian

$$H = - \sum_i \left[ (\sigma_i^+ \sigma_{i+1}^- + \sigma_i^- \sigma_{i+1}^+) + \frac{\Delta}{2} \sigma_i^z \sigma_{i+1}^z + h_i \sigma_i^z \right], \quad (7)$$

where  $\sigma_i^\pm = \sigma_i^x \pm i \sigma_i^y$ ,  $\Delta$  is the interaction strength, and  $h_i$  is a random magnetization. We take  $\Delta = 1$  and the field uniformly random  $h_i = [-W, W]$ . This model is often used to study the nature of the many-body localization (MBL) phase transition [10, 19]. The critical value of disorder in the literature is  $W_c \approx 3.8$  obtained through large-scale ( $L = 26$ ) exact diagonalization [26]. In the ergodic phase (small  $W$ ), the excited states have volume law entanglement. In the MBL phase (large  $W$ ), the spins are mostly weakly entangled, but the entanglement structure is the object of our interest. Clusters (of spins) are defined as a subsystem that has stronger entanglement internally than with the rest of the system.

Using exact diagonalization, we select  $k = 50$  eigenstates from the middle of the spectrum for  $N_d = 2000$  disorder realizations. For each eigenstate, we construct a Vietoris-Rips complex with the distance metric of Equation 2. The resulting persistence barcodes are merged by discarding the information from which realization each barcode originated. Since this leads to barcodes with many bars, we use Betti numbers (Equation 5) to summarize and investigate the results. Figure 7 shows the Betti numbers for varying disorder strengths  $W$ . As the disorder strength  $W$  decreases, there are fewer connected components as counted by the normalized  $\beta_0$ . The number of 1-cycles as counted by the normalized  $\beta_1$  is highest for  $W = 3.3$ .

Figure 8 shows the maximum of  $\beta_1$  (see Fig. 7) for varying disorder strength  $W$ . This maxima occur at a length scale around  $\epsilon \approx 0.95 \cdot 2 \ln 2$ . The Betti number

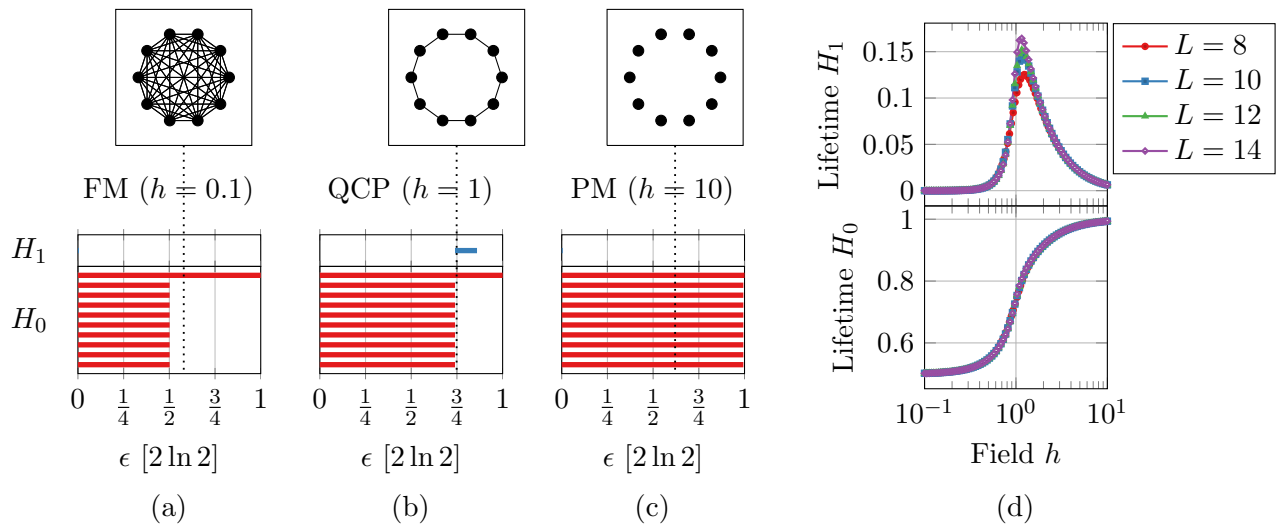


FIG. 5. Barcodes for transverse-field Ising chain with 10 sites at (a)  $h = 0.1$ , (b) 1 and (c) 10. The proximity parameter  $\epsilon$  refers to the length scale set by the distance matrix  $D(i, j)$ . At the quantum critical point, the spin chain forms a cycle of entanglement with a 1-dimensional hole. (d) Lifetime of  $H_1$  and  $H_0$  bars. The persistence of the 1-cycle at the QCP increases with system size  $L$ .

$\beta_1$  essentially counts the number of spin clusters that are more strongly entangled (strength set by  $\epsilon$ ) within the cluster than the environment. The minimum set of spins to form a 1-cycle is four spins (because three connected spins would form a 2-simplex in a Vietoris-Rips complex).

## VII. DISCUSSION

Computing the entanglement entropy of all possible partitions is numerically impractical due to the factorial number of possibilities. For single pairs of  $N$  particles (or spins), the number is " $N$  choose 2" (scales as  $O(N^2)$ ). However, due to the non-additivity of entropy, this does not necessarily capture all the structure present in the entanglement of the state.

Rather than starting from individual spins, it is also possible to perform a recursive bipartitioning of the spin chain (as used in [10]). This turns the wave function into a binary tree, where each node is a set of spins. Compared to our method, which is bottom-up from spin pairs,

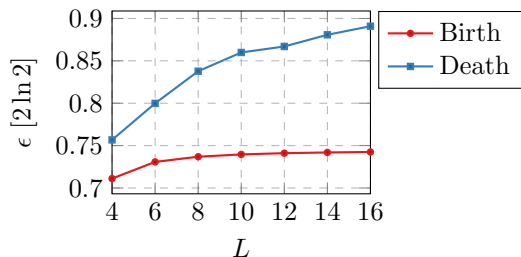


FIG. 6. Birth and death of the  $H_1$  persistence bar at the quantum critical point  $h = 1$  of the transverse-field Ising chain of varying size  $L$ .

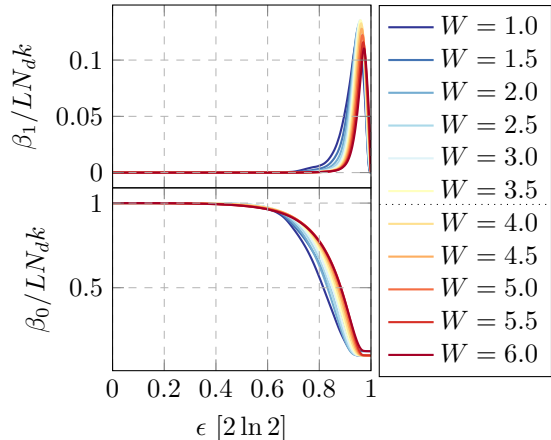


FIG. 7. Betti numbers  $\beta_0$  and  $\beta_1$  for varying disorder strength  $W$ . XXZ spin chain with  $L = 10$  sites,  $N_d = 2000$  realizations and  $k = 50$  states. The critical strength of a large-scale diagonalization study has predicted the phase transition to be at  $W_c \approx 3.8$  [26], this is marked by a dotted line in the legend.

this could be considered a top-down approach. Given the binary tree, the distance between leaf nodes (single spins) can be used to compute homology. This would be an alternative to our bottom-up approach based on mutual information and an interesting direction to explore in the future.

We compute entanglement entropy using singular value decomposition (SVD), but diagonalizing the partial trace of a density matrix (constructed as the outer product of the pure state) has similar computational complexity. The purity (or linear entropy) of a quantum state could be an alternative to the von Neumann entropy that is used here, and it has the benefit of not requiring diago-

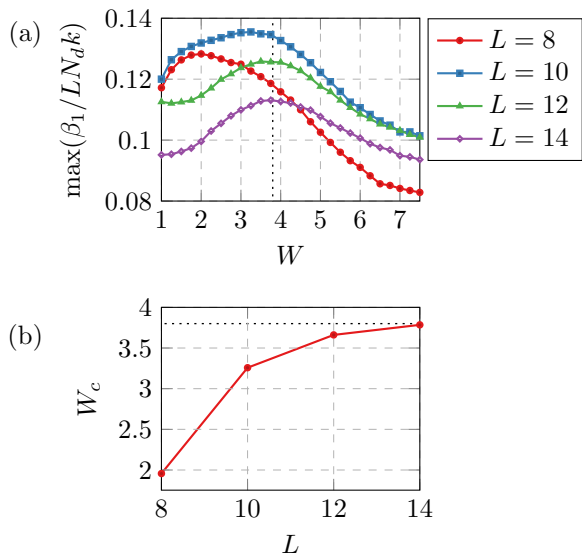


FIG. 8. (a) Maximum Betti number of the first homology group for varying disorder strength  $W$ . 1500 disorder realizations (b) The disorder strength with largest Betti number, i.e. peak in (a), this coincides with the expected critical strength of  $W_c \approx 3.8$  from large-scale exact diagonalization (marked by dotted line) [26].

nalization of the density matrix.

The first example of the Ising chain discussed in this paper can be solved efficiently using the Jordan-Wigner transformation. However, this is a special case, and it is not generally efficient for all interacting Hamiltonians, so we do not rely on this transformation in this work.

The von Neumann entropy is typically not experimentally accessible, whereas the Rényi entropy of order  $\alpha = 2$  is experimentally accessible in certain setups [27]. This would make it possible to compute the barcode of an experimental setup.

Regarding persistent homology, we note that our homology groups are computed with  $\mathbb{Z}_2$  (boolean) coefficients, the most common choice in topological data analysis. The choice of coefficients determines whether a simplex can occur multiple times in a chain or whether the direction of travel (represented by the sign of the coefficient) matters. The change in barcodes for entanglement structure when computing homology with different coefficients is also an interesting direction to explore.

TDA is a powerful tool that can be applied to the questions of emergent structures in the topology of the Hilbert space describing the system. This connects di-

rectly to a deeper question: does spacetime emerge from entanglement? This is one of the questions that is part of the Simons Collaboration: *It from Qubit* [28]. The study of the emergent geometry from entanglement is still a topic of active research [29–31]. For example, Cao *et al.* have proposed the use of mutual information and classical multidimensional scaling to form emergent geometry [32].

## VIII. CONCLUSION

Persistent homology is a useful tool for dealing systematically with the entanglement structure in quantum states. The topological features that it computes can be used to answer a number of scientific questions. First, the barcode of a quantum state changes dramatically when the state undergoes a quantum phase transition. It is therefore a new type of quantum order parameter. We have demonstrated its capability for two basic examples of the Ising chain and XXZ spin chain in a transverse field. Second, it can guide the development of suitable wave function ansätze, with for example tensor networks. Third, it provides a numerical approach for studying the emergent geometry of entanglement. This is very relevant to the scientific question whether spacetime emerges from entanglement.

The focus in this multidisciplinary work is on the application of persistent homology to quantum phase transitions, the first of the aforementioned uses of the method. However, it is possible to examine many quantum phenomena through the lens of homology and Betti numbers of the entanglement structure. The effect of adding time dependence to the presented scheme is also an promising future direction to explore.

## IX. ACKNOWLEDGEMENTS

The authors are grateful to Qian Yang, Loïc Herviou, Jens H. Bardarson and R. Matthias Geilhufe for discussions. We acknowledge funding from the VILLUM FONDEN via the Centre of Excellence for Dirac Materials (Grant No. 11744), the European Research Council ERC HERO-810451 grant, University of Connecticut, and the Swedish Research Council (VR) through a neutron project grant (BIFROST, Dnr. 2016-06955). The authors also acknowledge computational resources from the Swedish National Infrastructure for Computing (SNIC) at the High Performance Computing Centre North (HPC2N).

[1] M. B. Hastings, *Journal of Statistical Mechanics: Theory and Experiment* **2007**, P08024 (2007).  
 [2] F. Verstraete, M. M. Wolf, D. Perez-Garcia, and J. I. Cirac, *Physical Review Letters* **96** (2006), 10.1103/physrevlett.96.220601.  
 [3] G. Vidal, *Phys. Rev. Lett.* **101**, 110501 (2008).

[4] J. Eisert, M. Cramer, and M. B. Plenio, *Reviews of Modern Physics* **82**, 277 (2010).  
 [5] M. Srednicki, *Phys. Rev. Lett.* **71**, 666 (1993).  
 [6] C. Holzhey, F. Larsen, and F. Wilczek, *Nuclear Physics B* **424**, 443 (1994).

- [7] P. Calabrese and J. Cardy, *Journal of Statistical Mechanics: Theory and Experiment* **2004**, P06002 (2004).
- [8] A. Dutta, G. Aeppli, B. K. Chakrabarti, U. Divakaran, T. F. Rosenbaum, and D. Sen, *Quantum Phase Transitions in Transverse Field Spin Models* (Cambridge University Press, 2015).
- [9] B. Bauer and C. Nayak, *Journal of Statistical Mechanics: Theory and Experiment* **2013**, P09005 (2013).
- [10] L. Herviou, S. Bera, and J. H. Bardarson, *Physical Review B* **99** (2019), 10.1103/physrevb.99.134205.
- [11] E. P. L. van Nieuwenburg, Y.-H. Liu, and S. D. Huber, *Nature Physics* **13**, 435 (2017).
- [12] D. Zvyagintseva, H. Sigurdsson, V. K. Kozin, I. Iorsh, I. A. Shelykh, V. Ulyantsev, and O. Kyriienko, arXiv e-prints, arXiv:2104.12921 (2021), arXiv:2104.12921 [cond-mat.mes-hall].
- [13] I. Donato, M. Gori, M. Pettini, G. Petri, S. De Nigris, R. Franzosi, and F. Vaccarino, *Physical Review E* **93**, 052138 (2016).
- [14] Q. H. Tran, M. Chen, and Y. Hasegawa, “Topological Persistence Machine of Phase Transitions,” (2020), arXiv:2004.03169.
- [15] B. Olsthoorn, J. Hellsvik, and A. V. Balatsky, *Physical Review Research* **2** (2020), 10.1103/physrevresearch.2.043308.
- [16] A. Cole, G. J. Loges, and G. Shiu, “Quantitative and interpretable order parameters for phase transitions from persistent homology,” (2020), arXiv:2009.14231 [cond-mat.stat-mech].
- [17] H. Edelsbrunner, D. Letscher, and A. Zomorodian, in *Proceedings of the 41st Annual Symposium on Foundations of Computer Science, FOCS '00* (IEEE Computer Society, USA, 2000) p. 454.
- [18] A. Zomorodian and G. Carlsson, *Discrete Comput. Geom.* **33**, 249–274 (2005).
- [19] M. Žnidarič, T. Prosen, and P. Prelovšek, *Physical Review B* **77** (2008), 10.1103/physrevb.77.064426.
- [20] B. Olsthoorn, (2021), (Unpublished).
- [21] G. De Tomasi, S. Bera, J. H. Bardarson, and F. Pollmann, *Phys. Rev. Lett.* **118**, 016804 (2017).
- [22] E. Iyoda and T. Sagawa, *Phys. Rev. A* **97**, 042330 (2018).
- [23] N. Otter, M. A. Porter, U. Tillmann, P. Grindrod, and H. A. Harrington, *EPJ Data Science* **6** (2017), 10.1140/epjds/s13688-017-0109-5.
- [24] P. Bubenik, M. Hull, D. Patel, and B. Whittle, *Inverse Problems* **36**, 025008 (2020).
- [25] C. Maria, P. Dlotko, V. Rouvreau, and M. Glisse, in *GUDHI User and Reference Manual* (GUDHI Editorial Board, 2021) 3.4.1 ed.
- [26] F. Pietracaprina, N. Macé, D. J. Luitz, and F. Alet, *SciPost Physics* **5** (2018), 10.21468/scipostphys.5.5.045.
- [27] T. Brydges, A. Elben, P. Jurcevic, B. Vermersch, C. Maier, B. P. Lanyon, P. Zoller, R. Blatt, and C. F. Roos, *Science* **364**, 260 (2019).
- [28] “It from qubit: Simons collaboration on quantum fields, gravity and information,” <https://www.simonsfoundation.org/mathematics-physical-sciences/it-from-qubit/>, accessed: 2021-06-21.
- [29] S. M. Carroll, arXiv e-prints (2021), arXiv:2103.09780 [quant-ph].
- [30] A. Ney, in *Philosophy Beyond Spacetime*, edited by C. Wüthrich, B. L. Bihan, and N. Huggett (Oxford: Oxford University Press, 2020).
- [31] S. S. Roy, S. N. Santalla, J. Rodríguez-Laguna, and G. Sierra, in *Quantum Theory and Symmetries* (Springer International Publishing, 2020) pp. 347–357.
- [32] C. Cao, S. M. Carroll, and S. Michalakis, *Physical Review D* **95** (2017), 10.1103/physrevd.95.024031.
- [33] J. Preskill, *California Institute of Technology* **16**, 10 (1998).
- [34] E. H. Lieb and M. B. Ruskai, *Journal of Mathematical Physics* **14**, 1938 (1973).

## Appendix A: Bipartite entanglement entropy

The distance metric used in our work is based on quantum mutual information and the properties of entanglement entropy. We therefore recall the key properties of entanglement entropy. Bipartite entanglement entropy is computed by performing Schmidt decomposition on a quantum state. We start by breaking down the Hilbert space in two parts  $\mathcal{H} = \mathcal{H}_A \otimes \mathcal{H}_B$ , and form a matrix  $C_{ij}$  such that,

$$|\psi\rangle = \sum_{i=1} \sum_{j=1} C_{ij} |i\rangle_A \otimes |j\rangle_B, \quad (\text{A1})$$

where  $\{|i\rangle_A\}$  and  $\{|j\rangle_B\}$  are the basis sets for  $\mathcal{H}_A$  and  $\mathcal{H}_B$ , respectively [33]. Schmidt decomposition is essentially singular value decomposition  $\mathbf{C} = \mathbf{U}\mathbf{\Sigma}\mathbf{V}^\dagger$  where  $\lambda_\alpha$  forms the diagonal of  $\mathbf{\Sigma}$ . Assuming  $N_B > N_A$ , then the state can be expressed in the following form:

$$|\psi\rangle = \sum_{\alpha}^{2^{N_A}} \lambda_{\alpha} |\alpha\rangle_A \otimes |\alpha\rangle_B \quad (\text{A2})$$

If there are more than one non-zero singular values  $\lambda_{\alpha}$ , then the state is entangled. The singular values can also be used to compute the entanglement entropy

$$S = - \sum_j |\lambda_j|^2 \ln(|\lambda_j|^2) \quad (\text{A3})$$

which is zero if the state  $|\psi\rangle$  is a product state (without entanglement). It is also upper bounded to  $\ln(d)$  where  $d$  is the Hilbert space dimension. This is  $N \ln 2$  in case of  $N$  spins. Two other properties of quantum entropy that are used to form the distance metric are the triangle inequality,

$$|S_i - S_j| \leq S_{ij} \leq S_i + S_j, \quad (\text{A4})$$

and strong subadditivity [34],

$$S_x + S_z \leq S_{xy} + S_{yz}. \quad (\text{A5})$$

In the main text we show how the bipartite von Neumann entanglement entropy  $S$  is used to compute mutual information between subsystems and how it sets the length scale for the corresponding persistence barcodes.